Supporting Information

Exsolution of metal nanoparticles by control of point defects

Andreas Rosnes[1], Bo Jiang[2], Holger von Wenckstern[1], Øystein Prytz[1], Jonathan M. Polfus[2,*]

[1] Department of Physics, Centre for Materials Science and Nanotechnology, University of Oslo, PO Box 1048 Blindern, NO NO-0316 Oslo, Norway

[2] Department of Chemistry, Centre for Materials Science and Nanotechnology, University of Oslo, PO Box 1033 Blindern, NO-0315 Oslo, Norway

* Corresponding author E-mail: jonathan.polfus@kjemi.uio.no

Contents

1. Structural characterization and refinement (XRD)

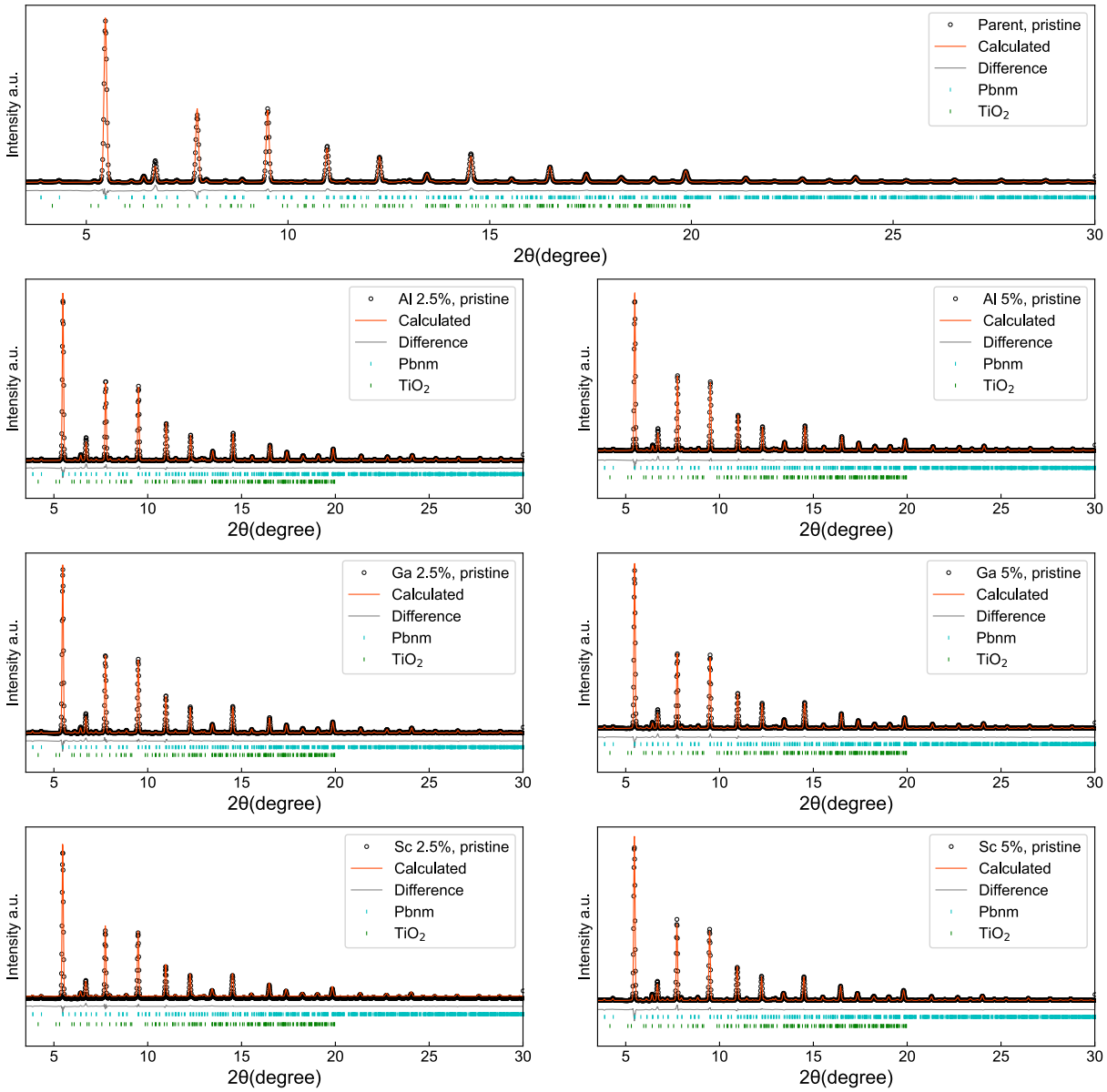

Figure S1. Rietveld refinements of synchrotron X-ray diffraction ex-situ data at room temperature for $La_{0.2}Ca_{0.7}Ti_{0.95}Cu_{0.05}O_{3-\delta}$ (parent) and $La_{0.2}Ca_{0.7}Ti_{0.95-x}Acc_xCu_{0.05}O_{3-\delta}$ (Acc = Al, Ga, Sc; x = 0.025, 0.05)

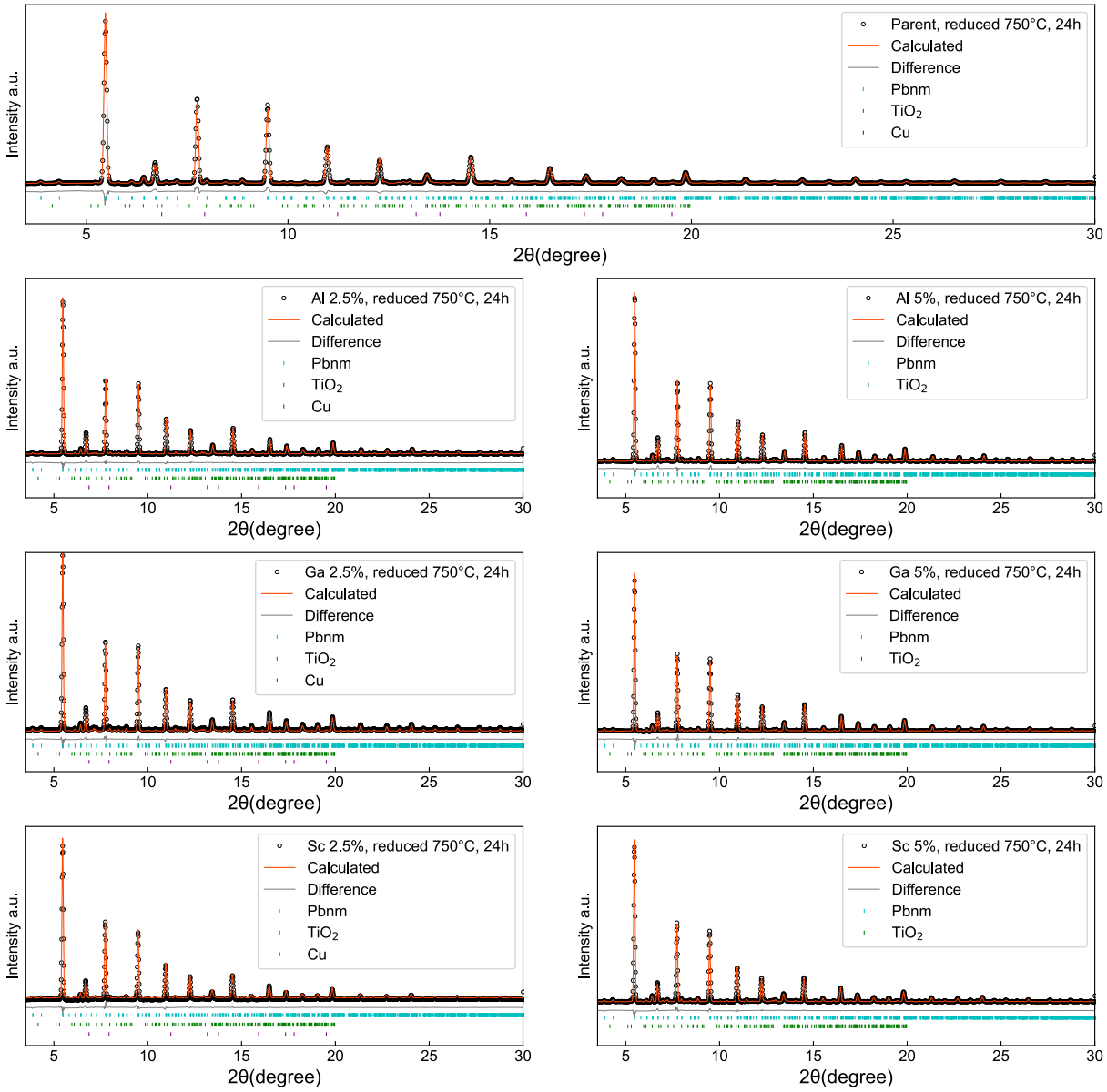

Figure S2. Rietveld refinements of synchrotron X-ray diffraction ex-situ data for $La_{0.2}Ca_{0.7}Ti_{0.95}Cu_{0.05}O_{3-\delta}$ (parent) and $La_{0.2}Ca_{0.7}Ti_{0.95-x}Acc_xCu_{0.05}O_{3-\delta}$ (Acc = Al, Ga, Sc; x = 0.025, 0.05) after exsolution at 750 °C for 24 hours in 5% H_2.

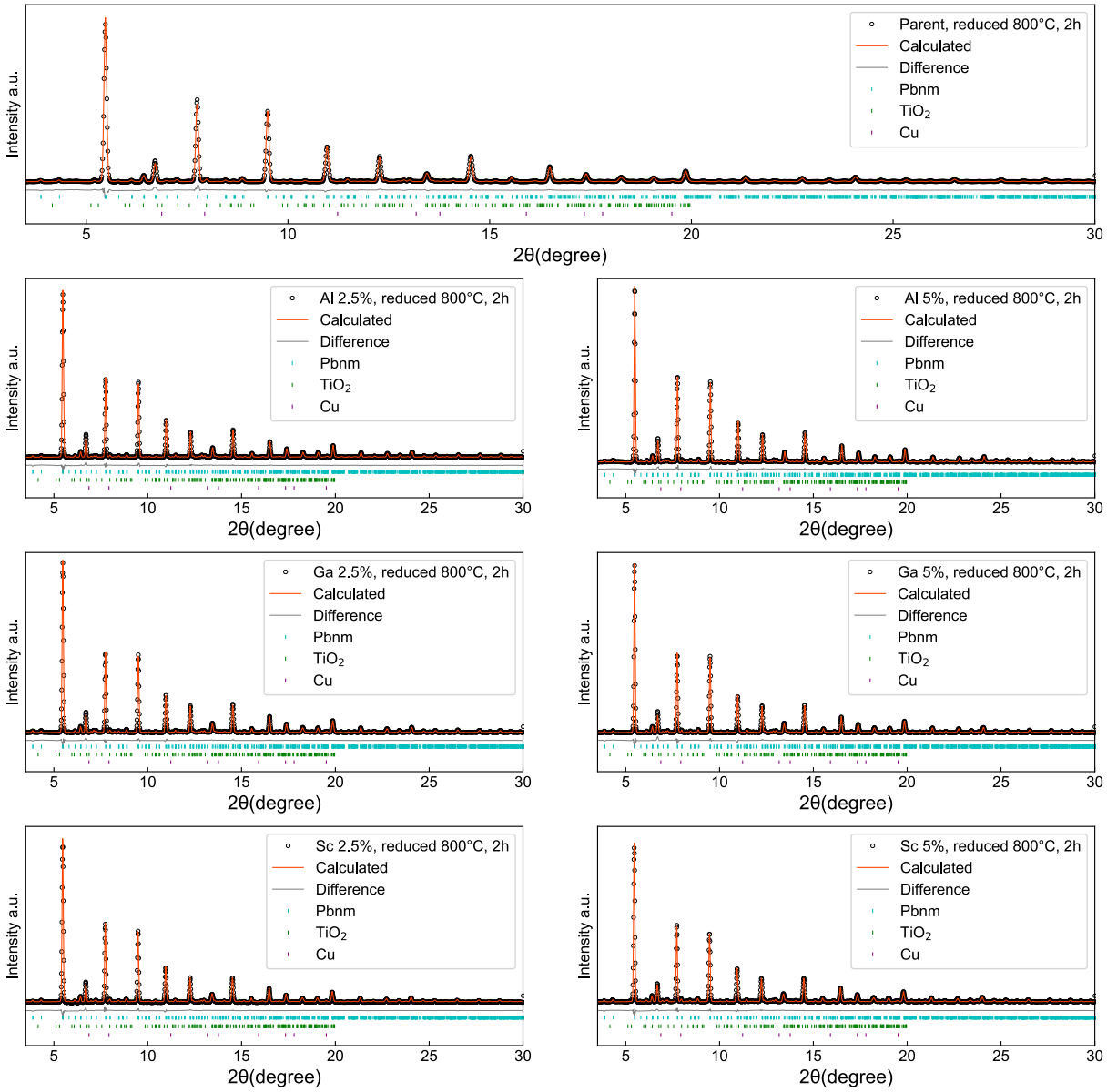

Figure S3. Rietveld refinements of synchrotron X-ray diffraction ex-situ data for $La_{0.2}Ca_{0.7}Ti_{0.95}Cu_{0.05}O_{3-\delta}$ (parent) and $La_{0.2}Ca_{0.7}Ti_{0.95-x}Acc_xCu_{0.05}O_{3-\delta}$ (Acc = Al, Ga, Sc; x = 0.025, 0.05) after exsolution at 800 °C for 2 hours in 5% H_2.

Table S1. Results of the Rietveld refinements of ex-situ data at room temperature for $La_{0.2}Ca_{0.7}Ti_{0.95}Cu_{0.05}O_{3-\delta}$ (parent) and $La_{0.2}Ca_{0.7}Ti_{0.95-x}Acc_xCu_{0.05}O_{3-\delta}$ (Acc = Al, Ga, Sc; x = 0.025, 0.05) before and after exsolution.

Sample	**R_{wp}**	**a** (Å)	**b** (Å)	**c** (Å)	**Pbnm** (wt.%)	**TiO_2** (wt.%)	**Cu** (wt.%)	**Cu** (mol%)
Pristine								
Parent	2.53	5.4231(3)	5.4489(3)	7.6829(4)	99.0(1)	1.04(13)	0	0
Ga 2.5%	1.90	5.4211(2)	5.4462(2)	7.6809(3)	99.9(1)	0.14(09)	0	0
Ga 5%	1.92	5.4217(2)	5.4479(2)	7.6827(3)	99.9(1)	0.07(10)	0	0
Al 2.5%	2.06	5.4164(3)	5.4373(3)	7.6742(5)	100.0(1)	0.03(11)	0	0
Al 5%	2.05	5.4157(3)	5.4384(3)	7.6743(4)	99.9(1)	0.06(11)	0	0
Sc 2.5%	1.84	5.4293(2)	5.4574(2)	7.6933(3)	99.7(1)	0.28(09)	0	0
Sc 5%	2.00	5.4343(2)	5.4658(2)	7.7030(3)	99.9(1)	0.12(10)	0	0
Reduced 750 °C, 24 h								
Parent	2.37	5.4231(3)	5.4476(3)	7.6838(5)	99.1(1)	0.71(12)	0.22(3)	10.5(16)
Ga 2.5%	1.80	5.4244(2)	5.4470(2)	7.6844(3)	99.2(1)	0.17(09)	0.59(3)	28.2(13)
Ga 5%	2.06	5.4226(3)	5.4455(2)	7.6852(4)	99.5(1)	0.17(11)	0.35(3)	16.8(13)
Al 2.5%	1.72	5.4177(3)	5.4371(2)	7.6762(4)	99.6(1)	0.08(09)	0.29(2)	13.8(10)
Al 5%	1.90	5.4166(3)	5.4366(2)	7.6762(4)	99.4(1)	0.25(10)	0.39(3)	18.4(12)
Sc 2.5%	2.26	5.4274(3)	5.4536(3)	7.6907(4)	99.6(1)	0.13(12)	0.24(3)	11.3(13)
Sc 5%	1.78	5.4350(2)	5.4640(2)	7.7051(3)	99.3(1)	0.38(09)	0.34(2)	15.9(11)
Reduced 800 °C, 2 h								
Parent	2.12	5.4226(3)	5.4493(3)	7.6842(4)	98.7(1)	1.16(11)	0.17(3)	7.9(12)
Ga 2.5%	1.61	5.4221(2)	5.4464(2)	7.6824(3)	99.3(1)	0.15(08)	0.54(2)	25.5(10)
Ga 5%	1.90	5.4236(2)	5.4474(2)	7.6830(3)	99.4(1)	0.27(09)	0.36(3)	17.1(12)
Al 2.5%	1.80	5.4167(3)	5.4368(2)	7.6747(4)	99.6(1)	0.14(09)	0.31(2)	14.7(11)
Al 5%	1.81	5.4151(3)	5.4359(2)	7.6741(4)	99.4(1)	0.23(09)	0.41(2)	19.2(11)
Sc 2.5%	1.79	5.4287(2)	5.4572(2)	7.6946(3)	99.3(1)	0.54(09)	0.21(2)	9.7(10)
Sc 5%	1.60	5.4348(2)	5.4646(2)	7.7040(3)	99.3(1)	0.39(08)	0.35(2)	16.6(10)

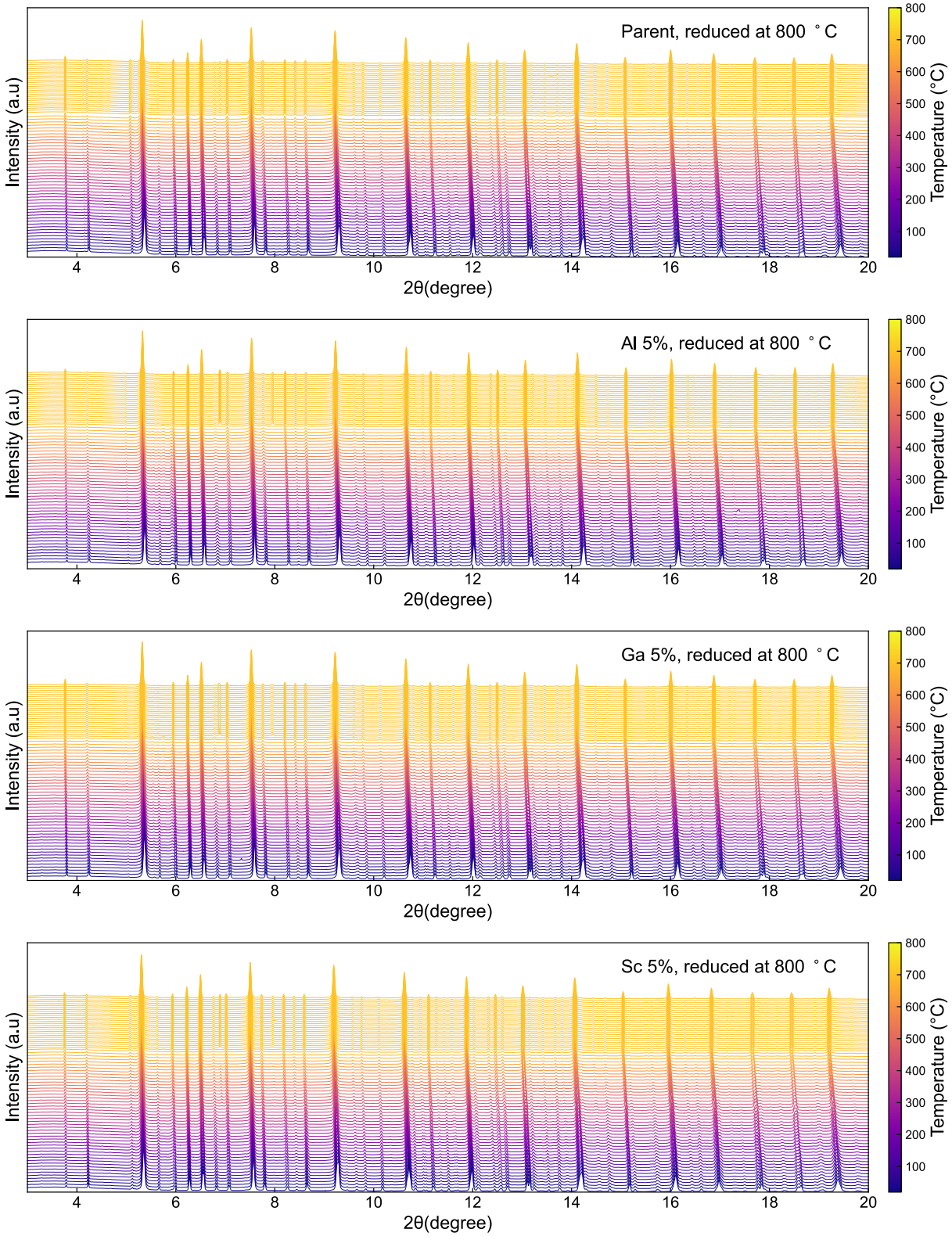

Figure S4. Stacked temperature-dependent XRD patterns in logarithmic scale for $La_{0.2}Ca_{0.7}Ti_{0.95}Cu_{0.05}O_{3-\delta}$ (parent) and $La_{0.2}Ca_{0.7}Ti_{0.9}Acc_{0.05}Cu_{0.05}O_{3-\delta}$ (Acc = Al, Ga, Sc) from RT to 800 °C, and then exsolved at 800 °C in 5% H_2.

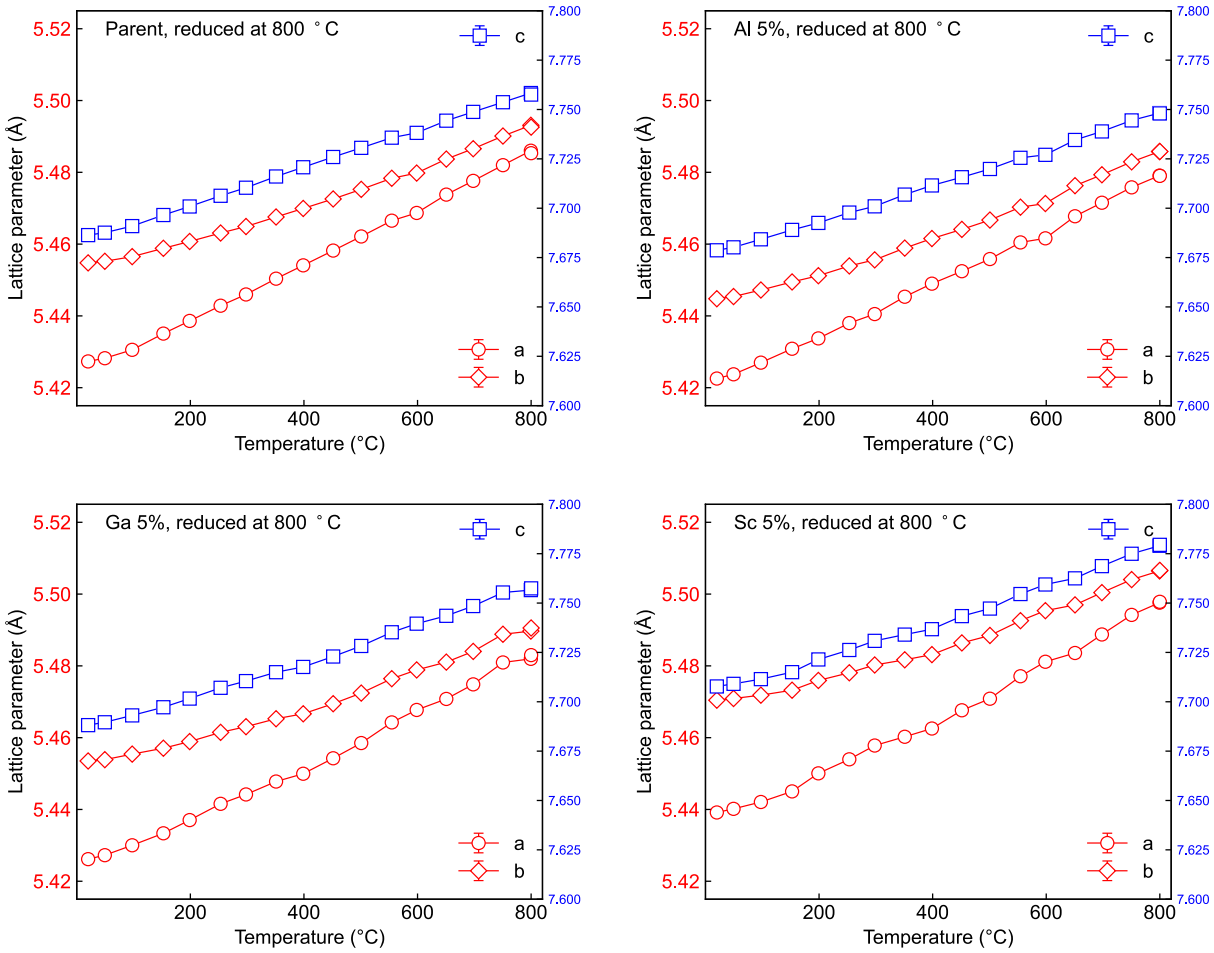

Figure S5. Temperature-dependent evolution of lattice parameters up to 800 °C in air for $La_{0.2}Ca_{0.7}Ti_{0.95}Cu_{0.05}O_{3-\delta}$ and $La_{0.2}Ca_{0.7}Ti_{0.95-x}Acc_xCu_{0.05}O_{3-\delta}$ (Acc = Al, Ga, Sc; x = 0.025, 0.05).

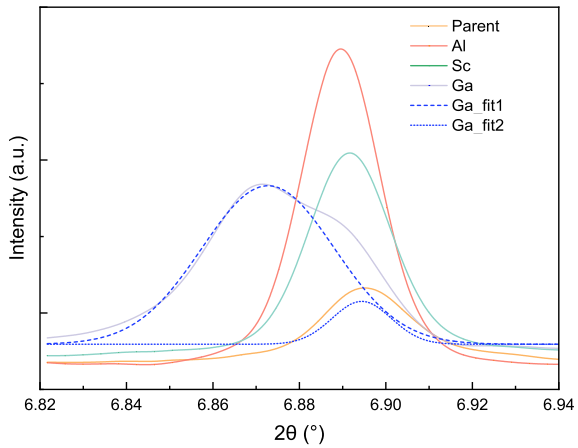

Figure S6. The Cu (111) peak at the end of exsolution during in situ XRD at 800 °C (120 min) for $La_{0.2}Ca_{0.7}Ti_{0.95-x}Acc_xCu_{0.05}O_{3-\delta}$ with Al, Sc, Ga x = (0, 0.05) with two gaussian fits highlighting strained particles in the Ga substituted sample.

The exsolution reaction for the parent sample can be described:

$$La_{0.2}Ca_{0.7}Ti_{0.95}Cu_{0.05}O_{2.95} \rightarrow La_{0.2}Ca_{0.7}Ti_{0.95}Cu_{0.05-x}O_{2.95-x} + xCu(s) + \frac{x}{2}O_2(g) \quad (1)$$

After complete exsolution, i.e., $x = 0.05$, the final weight fraction of the exsolved Cu X_f can be expressed:

$$X_f = \frac{0.05\ MW_{Cu}}{0.05\ MW_{Cu} + MW_{LCT}} \quad (2)$$

where the MW_{LCT} is the molecular weight of the host after exsolution, i.e., without copper and with the corresponding amount of oxygen loss according to Equation 1. The mole fraction of exsolved Cu throughout the in situ experiment was obtained from the weight fraction of Cu obtained from Rietveld refinement (X) relative to the final weight fraction:

$$\frac{x}{0.05} = \frac{X}{X_f} \quad (3)$$

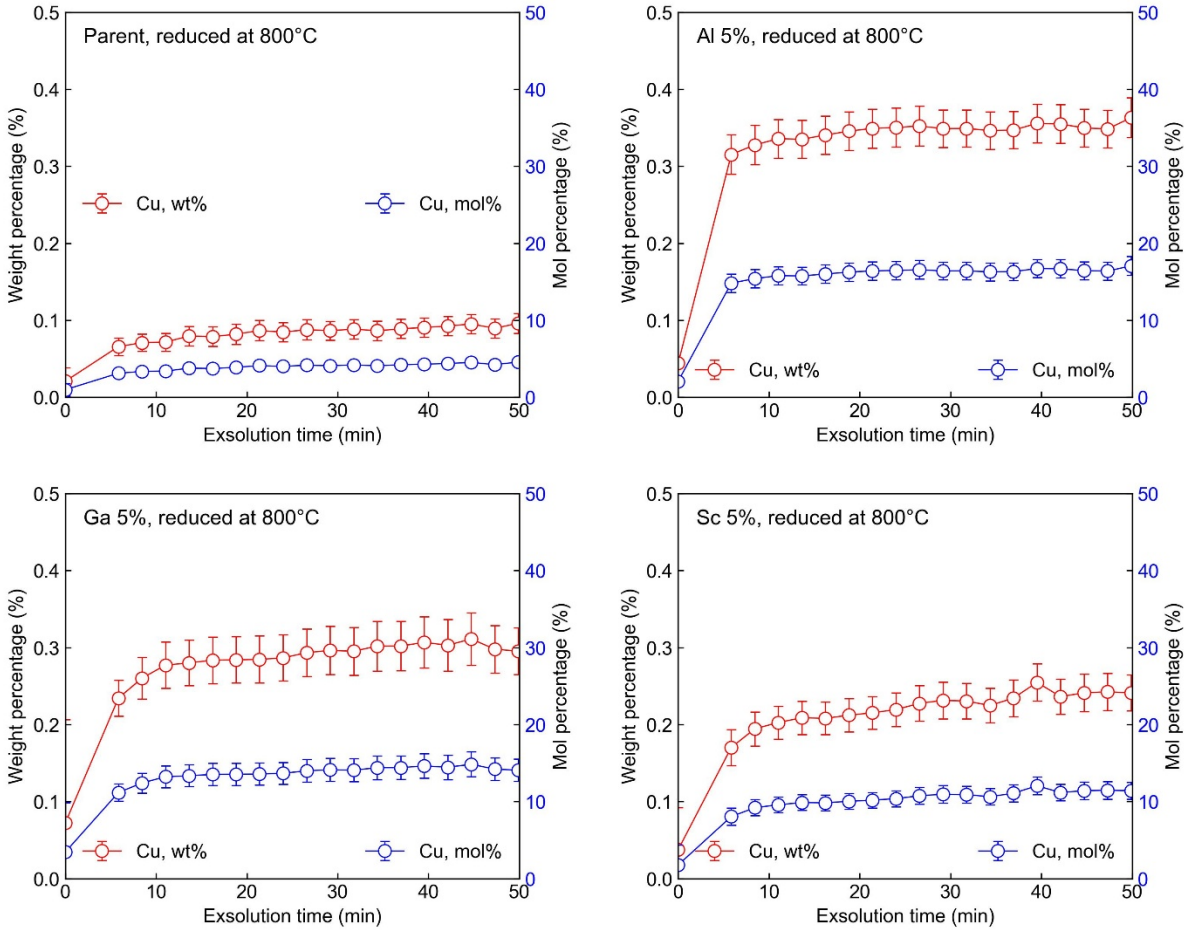

Figure S7. Evolution of the amount of exsolved copper from Rietveld refinement during exsolution at 800 °C in 5% H_2.

2. Quantification of cation stoichiometry (STEM-EDS)

The cation compositions of the pristine samples were quantified using scanning transmission electron microscopy energy-dispersive X-ray spectroscopy (STEM-EDS) prior to the reductive treatment. The quantification agrees with the nominal stoichiometry $La_{0.2}Ca_{0.7}Ti_{0.95-x}Acc_xCu_{0.05}O_{3-\delta}$ (x = 0, 0.05) within the uncertainty for the parent and acceptor substituted samples (Table 2). The values are normalized to the B-site and a statistically weighted average from five similar regions were combined to the final values. The EDS analysis is exemplified for $La_{0.2}Ca_{0.7}Ti_{0.9}Al_{0.05}Cu_{0.05}O_{3-\delta}$ in Figure S8 with STEM LAADF and atomic weighted elemental maps. The spectral image was smoothed using a moving average of a 9 pixel window prior to summation of the spectra to obtain a single spectrum with sufficient counts for reliable quantification. A multipolynomial background of second order, Schreiber-Wims ionization cross-section suited for metal oxides[1], and an optimized spectra fit within the Velox software were employed to obtain the cation stoichiometry.

Rietveld refinement shows that the parent sample contains a larger amount of the TiO_2 secondary phase (1.04 wt%) compared to the acceptor substituted samples (0.03–0.28 wt%) (Table S1). Accordingly, the EDS analysis indicates a slightly lower A-site deficiency for the parent sample, $La_{0.21}Ca_{0.72}Ti_{0.95}Cu_{0.05}O_{3-\delta}$ (Table S2). The slightly lower A-site deficiency in the parent sample is not expected to significantly impact the exsolution behaviour due to excess of A-site vacancies (7–10 mol% compared to 5 mol% Cu). Notably, the higher exsolution yield of the acceptor substituted samples corresponds to a similar level of excess A-site vacancies as the parent sample.

Table S2. Cation stoichiometry of the pristine $La_{0.2}Ca_{0.7}Ti_{0.95-x}Acc_xCu_{0.05}O_{3-\delta}$ powders from STEM-EDS.

Sample	**Cation stoichiometry** (mol fraction)				
	La	Ca	Ti	Acc.	Cu
Parent	0.21±0.03	0.72±0.11	0.95±0.14	n/a	0.05±0.01
Aluminum	0.20±0.03	0.70±0.10	0.91±0.13	0.05±0.01	0.04±0.01
Gallium	0.21±0.03	0.68±0.09	0.91±0.13	0.06±0.01	0.04±0.01
Scandium	0.21±0.03	0.70±0.10	0.91±0.13	0.05±0.01	0.04±0.01

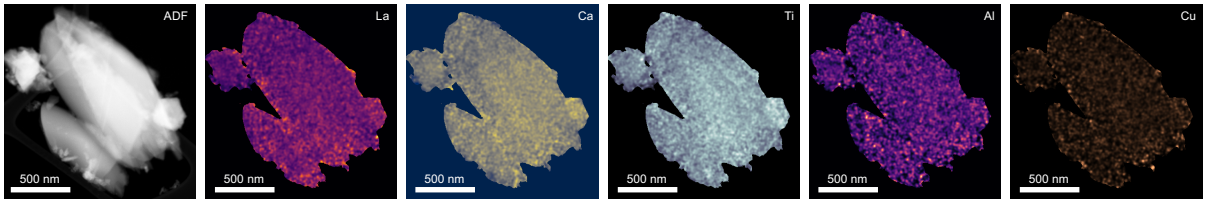

Figure S8. STEM-LAADF image and EDS elemental maps of La, Ca, Ti, Al, and Cu in $La_{0.2}Ca_{0.7}Ti_{0.9}Al_{0.05}Cu_{0.05}O_{3-\delta}$. The region outside the particle was masked for the visualization.

3. Quantification of copper charge states (XANES)

Linear combination fitting of the Cu K-edge spectra was used to quantify the relative amounts of the Cu(0), Cu(I), and Cu(II) oxidation states[2]. Figure S9 shows the ex situ XANES spectra used for quantification of the amount of exsolved copper in Figure 3a, overlayed with the best linear combination fit, residual, and the weighted reference spectra. While there are inherent limitations with the use of the Cu2O and CuO reference spectra due to the different chemical environments of Cu in the perovskite, the majority of Cu is in the metallic state corresponding to the Cu foil reference. The fitting residuals show no systematic mismatch to the spectra and the fitting uncertainties are minor (also given as error bars in Figure 1 and Figure 7).

The quantified amounts of the copper oxidation states throughout the in situ experiment are shown in Figure S10. The samples contain a minor amount of Cu(I) in air up to 800 °C, which is higher in the acceptor substituted samples. At the onset of the reductive treatment, there is an abrupt reduction of Cu(II) to predominately Cu(I) within the first minutes. In the parent sample, Cu(0) emerges after a delay of several minutes, while it appears instantaneously in the acceptor substituted samples in accordance with faster exsolution kinetics. The scandium substituted sample exhibits similarly fast exsolution kinetics at the onset, while the amount of Cu(0) and reduction to Cu(I) is lower than for the other acceptors due to the strain induced limitations. The corresponding fitting of selected XANES spectra is also presented in Figure S10. The discrepancies in the fitting may be ascribed to the difference in temperature and acquisition mode between the reference (transmission mode at 25° C) and in situ experiment (fluorescence mode at 800° C). Nevertheless, the linear combination fitting shows relatively small uncertainties (error bars in Figure 1d and Figure 7) and the quantification is validated by the overall agreement with the quantification of metallic copper from the Rietveld refinement of the XRD data (Figure 1c) with respect to time evolution and relative difference between the parent and acceptor substituted samples.

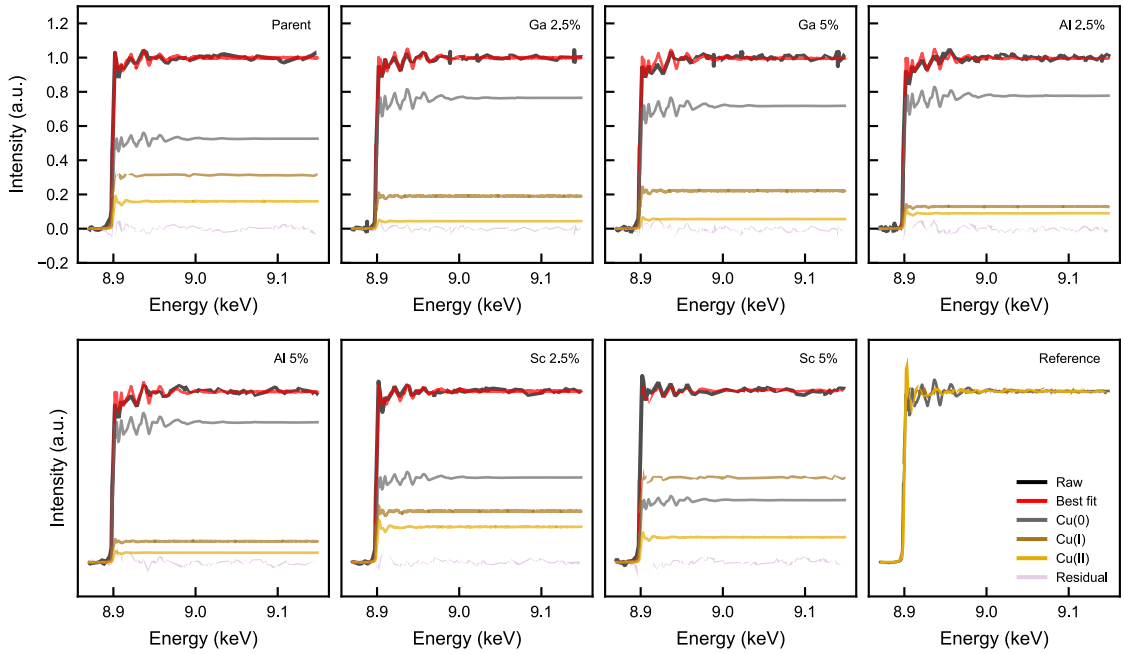

Figure S9. Linear combination fitting of ex situ XANES spectra of $La_{0.2}Ca_{0.7}Ti_{0.95-x}Acc_xCu_{0.05}O_{3-\delta}$ with aluminium and gallium ($x = 0$, 0.025, 0.05) after 24 hours at 750 °C used for quantifying the amount of exsolved metal in Figure 3a and Figure 7f.

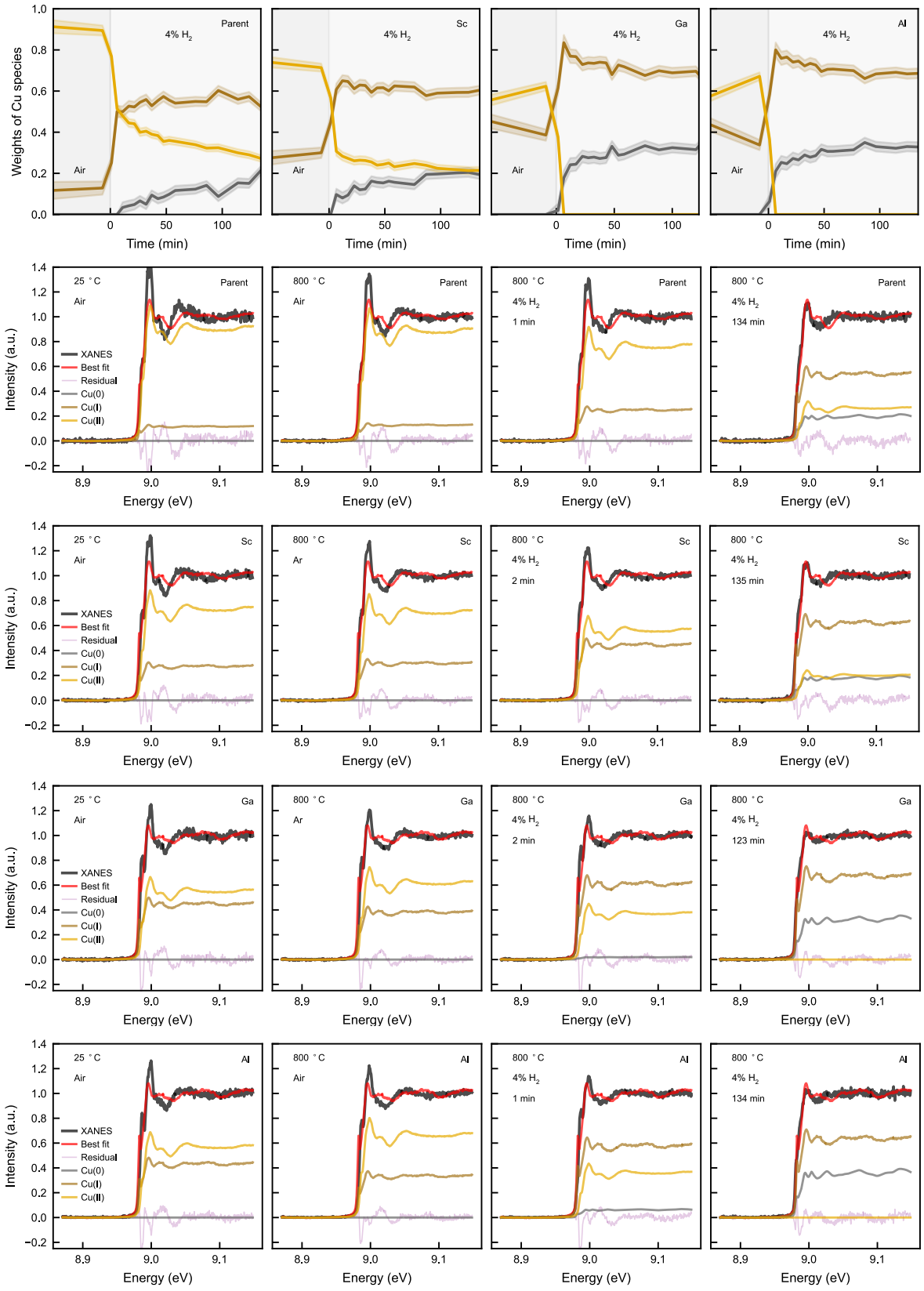

Figure S10. Quantified weights of Cu(0), Cu(I), and Cu(II) for the parent and acceptor substituted samples throughout the in situ experiment from linear combination fitting. The shaded area represents the error from goodness of fit. Linear combination fitting of selected XANES spectra from the in situ experiment for the parent and aluminum substituted sample at 25 °C and 800 °C in air, and at the onset (1 min) and end (134 min) of the reductive treatment.

4. Nanoscale imaging of particle populations (STEM)

STEM-ADF images used for the particle population analyses for samples reduced at 750 °C for 24 hours are presented Figure S11. The particle diameters were measured manually using the ImageJ software[3] for a population of 150 particles for each sample. The collection angles of the annular detector were optimized for phase contrast due to lattice imperfections in low angle annular dark-field (LAADF) imaging[4]. The coherent nature of the particles makes them otherwise challenging to detect using incoherent Z-contrast imaging, such as HAADF imaging, since the average atomic number is similar between regions with and without copper particles.

STEM-ADF images of samples reduced at 800 °C for 2 hours are presented in Figure S12.

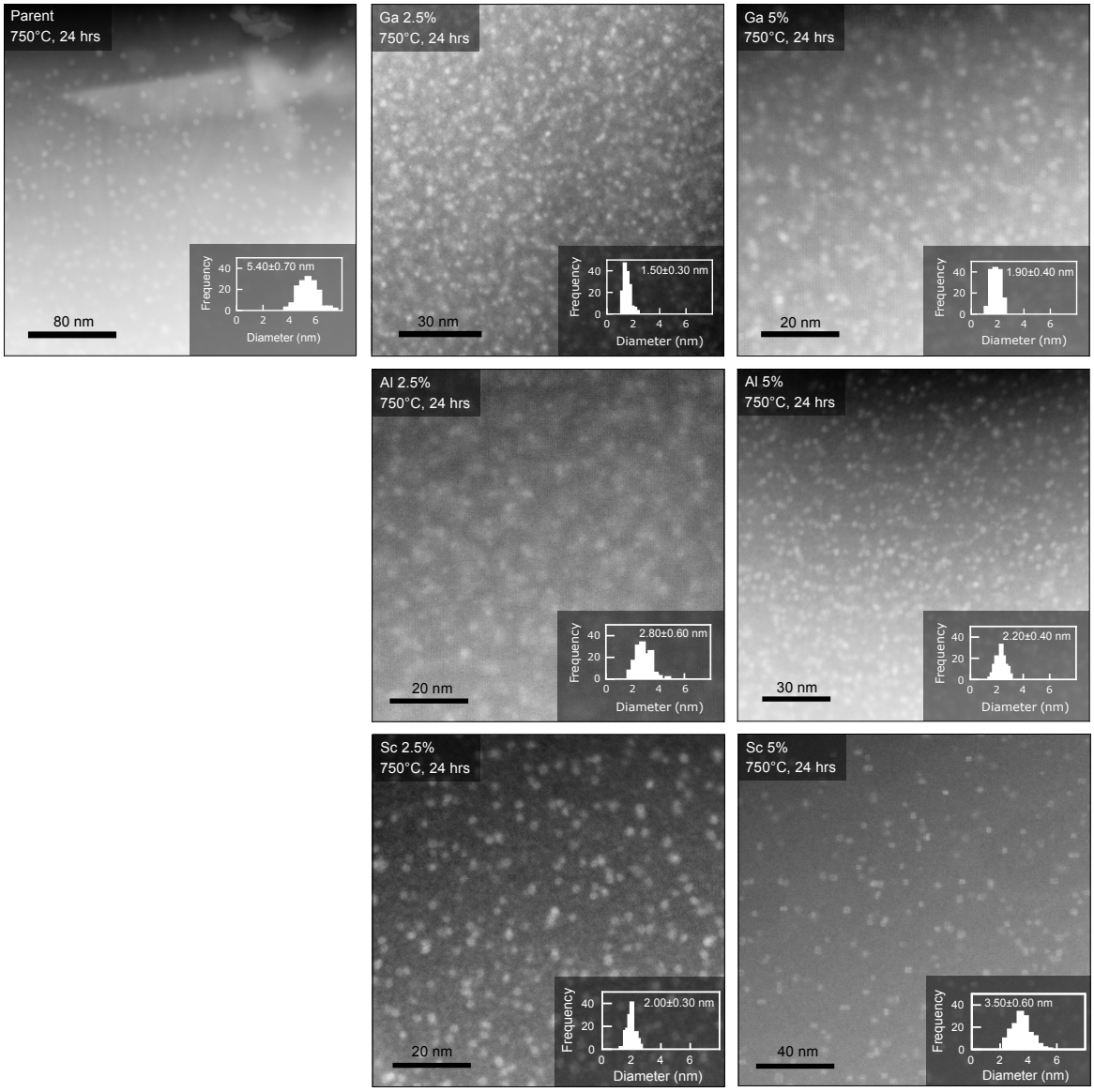

Figure S11. STEM-ADF images $La_{0.2}Ca_{0.7}Ti_{0.95-x}Acc_xCu_{0.05}O_{3-\delta}$ ($x = 0$, 0.025, 0.05) reduced at 750 °C for 24 hours and histograms of the size distributions of 150 nanoparticles with the mean diameter and standard deviation.

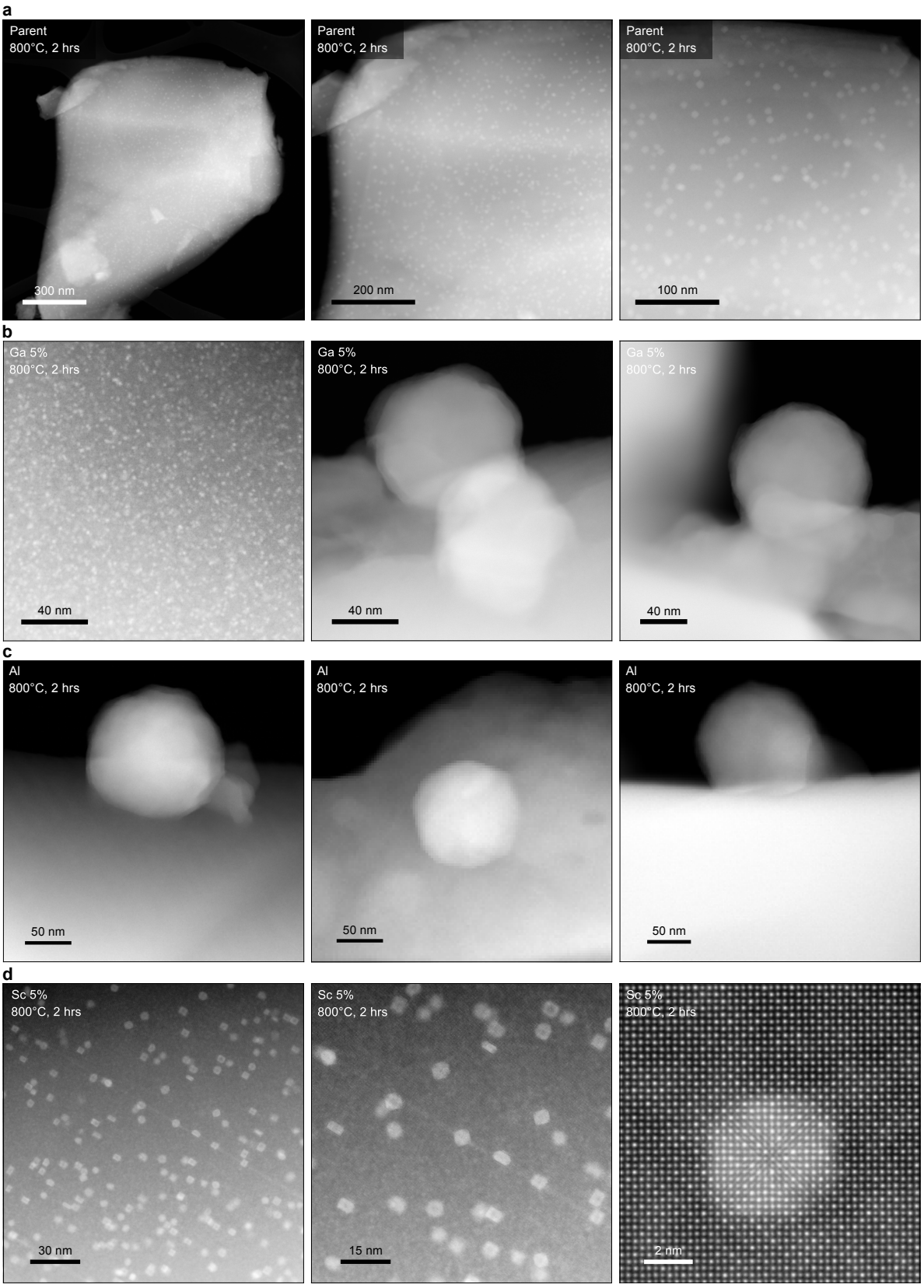

Figure S12. STEM-ADF images of $La_{0.2}Ca_{0.7}Ti_{0.95-x}Acc_xCu_{0.05}O_{3-\delta}$ (x = 0, 0.05) reduced at 800 °C for 2 hours: **a,** parent and substituted with acceptors **b,** Ga, **c,** Al and **d,** Sc.

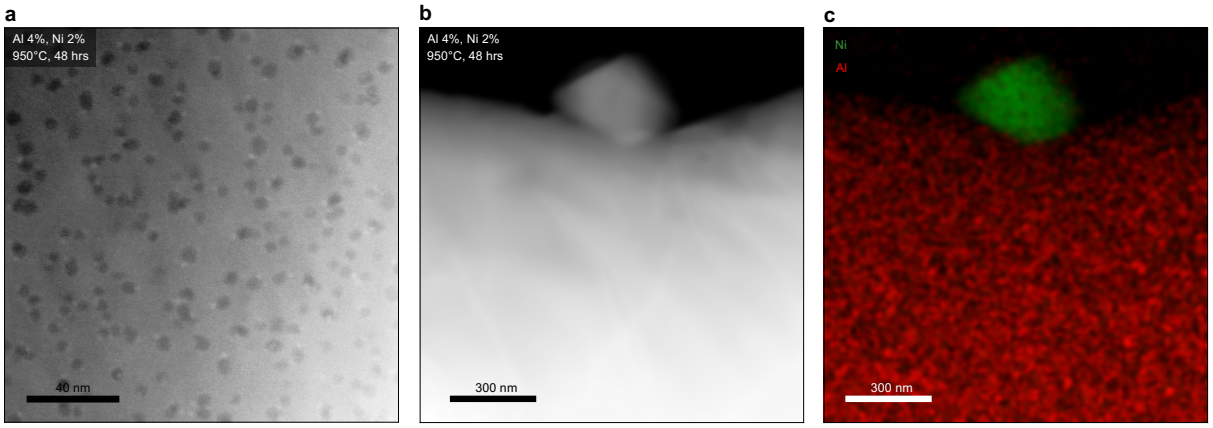

Figure S13. STEM-HAADF images (a, b) and EDS elemental map (c) of $La_{0.2}Sr_{0.7}Ti_{0.94}Al_{0.04}Ni_{0.02}O_{3-\delta}$ reduced at 950 °C for 48 hours.

5. Thermogravimetry (TG)

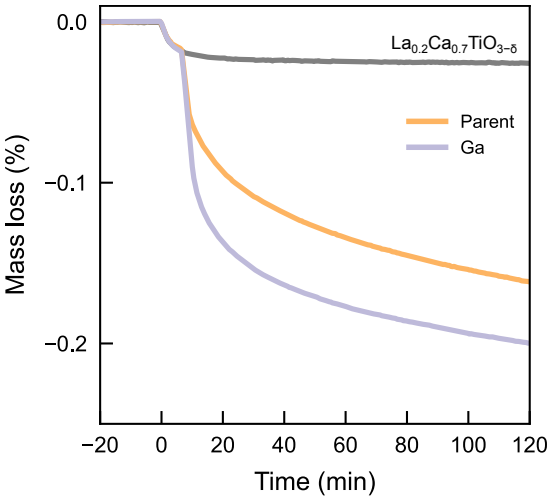

Figure S14. Thermogravimetric analysis of mass loss due to the release of oxygen at 800 °C after introducing 5% H_2 at time zero for $La_{0.2}Ca_{0.7}Ti_{0.9}Ga_{0.05}Cu_{0.05}O_{3-\delta}$. $La_{0.2}Ca_{0.7}TiO_{3-\delta}$ is used as a reference to show that the reduction is minor in absence of exsolution.

6. Processing of atomic scale energy loss spectra (STEM-EELS)

The electron energy loss spectroscopy (EELS) spectral image was obtained for a copper nanoparticle located in region of thickness below 25 nm (Figure 15a,b). The spectrum dispersion was optimized to cover an energy loss range encompassing the CaL (346 eV), TiL (456 eV), OK (532 eV), LaM (832 eV), CuL (931 eV), and GaL (1115 eV) edges. The edges are sufficiently separated (>50 eV) for proper background subtraction with minor influence from fine structure details in the extended region. The location of the A-, B-, and oxygen sites are known prior to the preprocessing due to simultaneous ADF imaging, which serves to verify the CaL, TiL, and OK elemental maps. While LaM precedes the CuL-edge, LaM the major sharp peaks associated with the M_4 and M_5 transitions and minor features in the extended regions enables robust background subtraction for the CuL-edge.

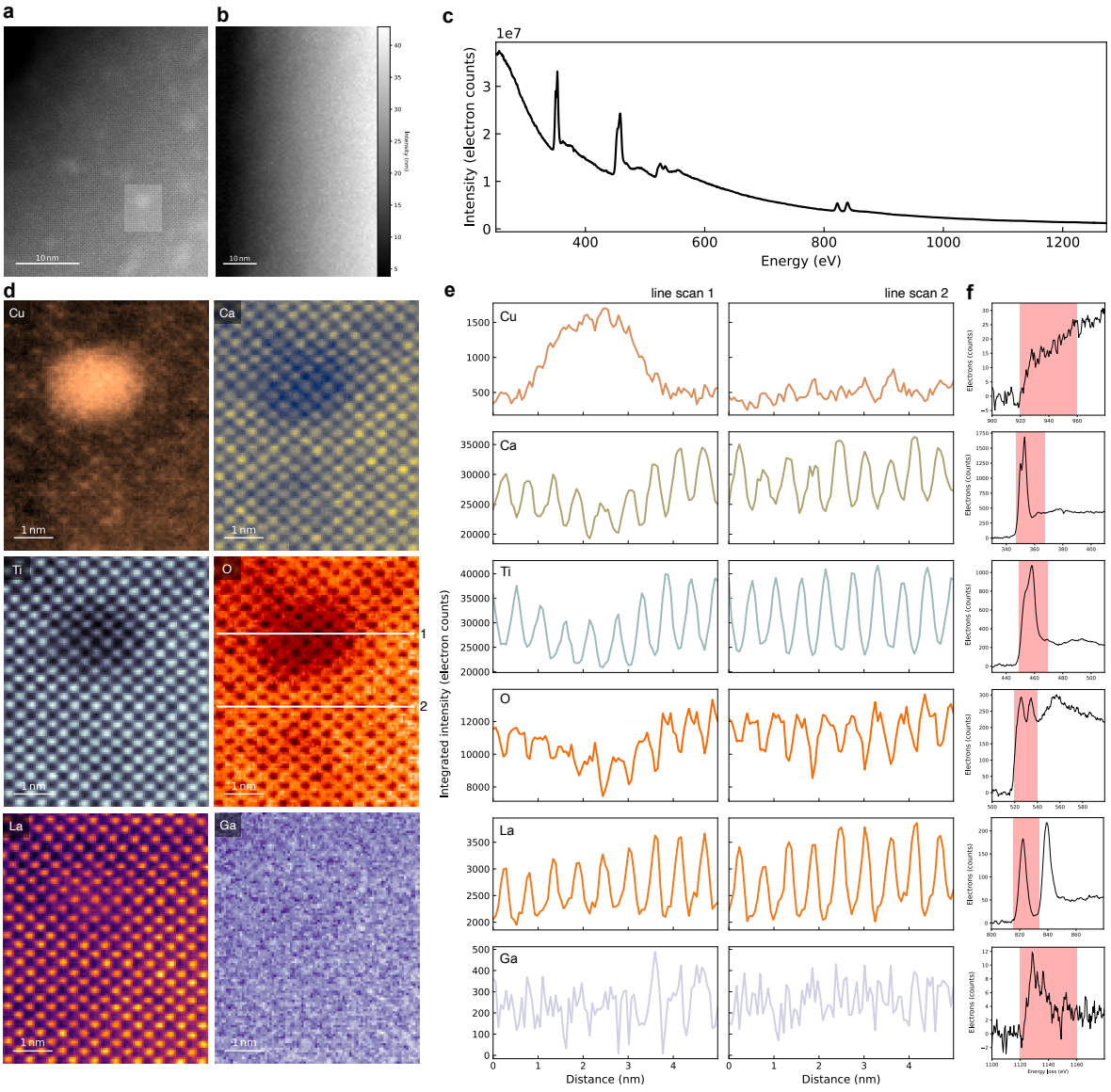

Figure S15. a, STEM ADF image showing the location of the spectral EELS image (shaded rectangle) close to the edge of the wedge in a region of uniform thickness (<25 nm) as obtained from the **b,** thickness map using the log-ratio method. **c,** Summed raw energy spectra encompassing the CaL (346 eV), TiL (456 eV), OK (532 eV), LaM (832 eV), CuL (931 eV), and GaL (1115 eV) edges. **d,** Elemental maps and **e,** line profiles across the copper nanoparticle (line scan 1) and across the host perovskite (line scan 2) show a lowered Ca, Ti, and O signal in place of the copper nanoparticle. The dashed lines in the OK map indicate the position of the line profiles. **f,** Single pixel spectra for the elemental edges with the integration window used for the map.

References

1. Schreiber, T. P. & Wims, A. M. A quantitative X-ray microanalysis thin film method using K-, L-, and M-lines. *Ultramicroscopy* **6**, 323–334 (1981).
2. Gaur, A., Shrivastava, B. D. & Joshi, S. K. Copper K-edge XANES of Cu(I) and Cu(II) oxide mixtures. *J. Phys.: Conf. Ser.* **190**, 012084 (2009).
3. Schneider, C. A., Rasband, W. S. & Eliceiri, K. W. NIH Image to ImageJ: 25 years of image analysis. *Nat Methods* **9**, 671–675 (2012).
4. Phillips, P. J. *et al.* Atomic-resolution defect contrast in low angle annular dark-field STEM. *Ultramicroscopy* **116**, 47–55 (2012).